Monthly Notices
of the
ROYAL ASTRONOMICAL SOCIETY

Mon. Not. R. Astron. Soc. **413,** 301–312 (2011) doi:10.1111/j.1365-2966.2010.18137.x

The geometry of the filamentary environment of galaxy clusters

Yookyung Noh[1] and J. D. Cohn[2]⋆

[1] *Department of Astronomy and Theoretical Astrophysics Center, University of California, Berkeley, CA 94720, USA*
[2] *Space Sciences Laboratory and Theoretical Astrophysics Center, University of California, Berkeley, CA 94720, USA*

Accepted 2010 December 1. Received 2010 November 30; in original form 2010 November 12

ABSTRACT

We construct a filament catalogue using an extension of the halo-based filament finder of Zhang et al. (2009), in a 250 Mpc h^{-1} side N-body simulation, and study the properties of filaments ending upon or in the proximity of galaxy clusters (within 10 Mpc h^{-1}). In this region, the majority of filamentary mass, halo mass and galaxy richness centred upon the cluster tends to lie in sheets, which are not always coincident. Fixing a sheet width of 3 Mpc h^{-1} for definiteness, we find the sheet orientations and (connected) filamentary mass, halo mass and richness fractions relative to the surrounding sphere. Filaments usually have one or more end points outside the sheet determined by filament or halo mass or richness, with at least one having a large probability to be aligned with the perpendicular of the plane. Scatter in mock cluster mass measurements, for several observables, is often correlated with the observational direction relative to these local sheets, most often for richness and weak lensing, somewhat less for Compton decrement and least often for velocity dispersions. The long axis of the cluster also tends to lie in the sheets and its orientation relative to the line of sight also correlates with mass scatter.

Key words: galaxies: clusters: general – cosmology: theory – large-scale structure of Universe.

1 INTRODUCTION

Large-scale structure in the Universe forms a cosmic web (Zel'dovich, Einasto & Shandarin 1982; Shandarin & Zel'dovich 1983; Einasto et al. 1984; Bond, Kofman & Pogosyan 1996), evident in the Universe's dark matter, halo, galaxy and gas distributions. The richness of the cosmic web is evident when one has sufficient statistics and resolution (numerically) or sensitivity (observationally) to see beyond the densest structures, correspondingly there has been a wealth of study of its properties. Examples include characterization of average properties (e.g. see Schmazling 1998 for one early review, Shandarin 2004, 2010; van de Weygaert et al. 2010 for some more recent papers and references within); identifying the web in observations and simulations (e.g. Bharadway et al. 2000; Pimbblet, Drinkwater & Hawkrigg 2004; Porter & Raychaudhury 2007; Feix et al. 2008; Porter et al. 2008; Sousbie et al. 2008a; Bond, Strauss & Cen 2010a; Bond, Strauss & Cen 2010b; Choi et al. 2010; Mead, King & McCarthy 2010; Murphy, Eke & Frenk 2010; Sousbie, Pichon & Kawahara 2010; Way, Gazis & Scargle 2010); tracing its relation to initial conditions (e.g. Shandarin, Habib & Heitmann 2009); and comparing filamentary environments and properties of galaxies within them (spin, shapes, alignments and more: Lee 2004; Altay, Colberg & Croft 2006; Dolag et al. 2006; Pandey & Somnath 2006; Aragón-Calvo et al. 2007b; Faltenbacher et al. 2007; Hahn et al. 2007a,b; Ragone-Figueroa & Plionis 2007; Lee et al. 2008; Paz et al. 2008; Betancort-Rijo & Trujillo 2009; Gay et al. 2009; Schäfer 2009; Zhang et al. 2009; Hahn, Teyssier & Carollo 2010; Jones, van de Weygaert & Aragón-Calvo 2010; Wang et al. 2010). Cluster alignments and formation, presumably or explicitly along filaments, have also been studied (e.g. van de Weygaert & Bertschinger 1996; Splinter et al. 1997; Colberg et al. 1999; Chambers, Melott & Miller 2000; Onuora & Thomas 2000; Faltenbacher et al. 2002; van de Weygaert 2002; Hopkins, Bahcall & Bode 2004; Bailin & Steinmetz 2005; Faltenbacher et al. 2005; Kasun & Evrard 2005; Lee & Evrard 2007; Lee et al. 2008; Pereira, Bryan & Gill 2008; Costa-Duarte, Sodre & Durret 2010), and several observed systems with filaments have been analysed in detail; some examples are found in Porter & Raychaudhury (2005), Gal et al. (2008), Kartaltepe et al. (2008) and Tanaka et al. (2009). Numerous methods for identifying filaments, suitable for different applications, have been proposed (for example, Barrow, Bhavsar & Sonoda 1985; Mecke, Buchert & Wagner 1994; Sahni, Sathyaprakash & Shandarin 1998; Schmalzing et al. 1999; Colombi, Pogosyan & Souradeep 2000; Sheth et al. 2003; Pimbblet 2005a,b; Stoica et al. 2005; Novikov, Colombi & Doré 2006; Aragón-Calvo et al. 2007a; Colberg 2007; van de Weygaert & Schaap 2007; Sousbie et al. 2008b; Stoica, Martinez & Saar 2007; Forero-Romero et al. 2009; Gonzalez & Padilla 2009; Pogosyan et al. 2009; Sousbie, Colombi & Pichon 2009; Stoica, Martinez & Saar 2009; Wu, Batuski & Khalil 2009; Genovese et al. 2010; Murphy, Eke & Frenk 2010;

⋆E-mail: jcohn@berkeley.edu

Shandarin 2010; Sousbie 2010; Way et al. 2010); see Zhang et al. (2009), Aragón-Calvo, van de Weygaert & Jones (2010b) for some comparisons of these. Analytic studies of filaments include estimates of their multiplicity (Lee 2006; Shen et al. 2006), anisotropy (e.g. Lee & Springel 2009), the merger rates of haloes into them (Song & Lee 2010) and properties in non-Gaussian theories (De Simone, Maggiore & Riotto 2010).

Galaxy clusters (dark matter haloes with mass $M \geq 10^{14}\, h^{-1}\, \mathrm{M}_{\odot}$) are of great interest for many reasons, in part because of their sensitivity to cosmological parameters, but also as hosts of the most massive galaxies in the Universe, as environments for galaxy evolution more generally and as the largest virialized objects in the Universe with correspondingly special astrophysical processes and histories (for a review, see e.g. Voit 2005). Galaxy clusters tend to lie at nodes of the cosmic web, with matter streaming into them from filaments (e.g. van Haarlem & van de Weygaert 1993; Diaferio & Geller 1997; Colberg et al. 1999). Although the Universe is isotropic and homogeneous on large scales, around any individual cluster there will be directionally dependent density fluctuations due to the condensation of filamentary and sheetlike matter around it. Our interest here is in characterizing this nearby (within $10\,\mathrm{Mpc}\,h^{-1}$) filamentary environment of galaxy clusters. This environment feeds galaxy clusters and is also unavoidably included for many observations of the cluster at its centre. This correlated environment is one source of the observationally well-known 'projection effects', which have plagued optical cluster finding starting with Abell (1958) and later (e.g. Dalton et al. 1992; Lumsden et al. 1992; van Haarlem, Frenk & White 1997; White et al. 1999); cluster weak lensing (e.g. Reblinsky & Bartelmann 1999; Hoekstra 2001; Metzler, White & Loken 2001; de Putter & White 2005; Becker & Kravtsov 2010; Meneghetti et al. 2010); cluster Sunyaev–Zel'dovich (Sunyaev & Zel'dovich 1972, 1980) (SZ) flux measurements (e.g. White, Hernquist & Springel 2002; Hallman et al. 2007; Holder, McCarthy & Babul 2007; Shaw, Holder & Bode 2008); and cluster velocity dispersions (e.g. Cen 1997; Tormen 1997; Kasun & Evrard 2005; Biviano et al. 2006). The environments of clusters have been studied within several contexts and using several methods, e.g. galaxy and dark matter density around clusters (Wang et al. 2009; Poggianti et al. 2010); filamentary growth (e.g. van de Weygaert 2006) around clusters; filamentary counts (Pimbblet et al. 2004; Colberg, Krughoff & Connolly 2005; Aragón-Calvo, van de Weygaert & Jones 2010b; Aragón-Calvo, Shandarin & Szalay 2010a), in particular the geometry and properties of superclusters (e.g. Shadarin, Sheth & Sahni 2004; Basilakos et al. 2006; Wray et al. 2006; Costa-Duarte, Sodre & Durret 2010); and the cluster alignment studies such as mentioned above.

Here we describe our findings on local cluster environments obtained by implementing the halo-based filament finder of Zhang et al. (2009) in a high-resolution N-body simulation. After refining the finder slightly for our purposes, we obtain a filament catalogue, and consider those filaments connected to or in the vicinity of galaxy clusters. Our work is most closely related to that of Colberg et al. (2005) and Aragón-Calvo et al. (2010b). They used simulations to measure counts of filaments (found via different algorithms) ending upon clusters and average filamentary profiles and curvature (observationally counts were found for the 2dFGRS data set in Pimbblet et al. 2004). We go beyond these to measure the statistics of the local geometry of filaments around their cluster end points. Related studies of filament geometry, particularly for superclusters, are found in e.g. Aragón-Calvo et al. (2010a,b); the former also discuss the tendency of filaments around voids and clusters to lie in sheets. We find that most of the filamentary (and halo) material in a $10\,\mathrm{Mpc}\,h^{-1}$ sphere around clusters lies in a plane, presumably the one from which the filaments collapsed, and investigate different ways of defining such a plane's orientation. Many measures of cluster masses include the cluster environment and as a result scatter the mass from its true value. In mock observations on simulations, we find that a line-of-sight-dependent scatter in measured cluster masses, for several methods, is often correlated with the angle between the line of sight and these locally defined planes.

In Section 2 we describe the simulations, mock observations and filament finder. In Section 3 we describe the statistical properties of the filaments and matter distribution around clusters In Section 4 we consider the geometry of the filament, mass and richness distributions within $10\,\mathrm{Mpc}\,h^{-1}$ of each cluster, focusing particularly on planes maximizing these quantities. In Section 5 we compare scatter in cluster masses to the orientation of observations with these planes, and in Section 6 we conclude.

2 SIMULATIONS AND METHODS

2.1 Simulation

We use a dark-matter-only simulation, in a periodic box of side $250\,\mathrm{Mpc}\,h^{-1}$ with 2048^3 particles evolved using the TREEPM (White 2002) code, and provided to us by Martin White. It is the same simulation as used in White, Cohn & Smit (2010) (hereafter WCS), which can be consulted for details beyond those found below. The background cosmological parameters are $h = 0.7$, $n = 0.95$, $\Omega_{\mathrm{m}} = 0.274$ and $\sigma_8 = 0.8$, in accord with a large number of cosmological observations. The simulation has outputs at 45 times equally spaced in $\ln(a)$ from $z = 10$–0. We focused on $z = 0.1$, in part to allow comparison with observational quantities in Section 5. Haloes are found using a Friends of Friends (FoF) halo finder (Davis et al. 1985), with linking length $b = 0.168$ times the mean interparticle spacing. Masses quoted below are FoF masses.

Resolved subhaloes in this high-resolution simulation are of importance for the observational comparisons in Section 5, and for measurements of galaxy properties in and around the clusters. Subhaloes are found via FoF6d (Diemand, Kuhlen & Madau 2006), with the specific implementation as described in the appendix of WCS. The subhaloes correspond to galaxies with luminosities $\geq 0.2L^*$ at $z = 0.1$,[1] and match observations as described in WCS. The halo and subhalo catalogues and dark matter particles can be combined to produce mock observations for six cluster mass measures. These are (see WCS for specifics and tests of the catalogue): two richnesses [one using the Koester et al. (2007) MAXBCG algorithm based upon colours,[2] and the other based upon spectroscopy, with cluster membership assigned via the criteria of Yang, Mo & van den Bosch 2008]; SZ flux or Compton decrement (flux within an annulus of radius r_{180b}, the radius within which the average mass is greater than or equal to 180 times background density); weak lensing (using an SIS or NFW model to assume a cluster lens profile and then fitting for a velocity dispersion and then mass); and two velocity dispersions (one based on a simple 3σ clipping, the other on a more complex method using phase-space information to reject outliers and calculating mass using a measured harmonic radius

[1] Approximately -18.5 in r band; see WCS for more discussion.

[2] Colour assignments are estimated using the prescription of Skibba & Sheth (2009) with evolution of Conroy, Gunn & White (2009), Conroy, White & Gunn (2010) and Conroy & Gunn (2010). Galaxies are taken to be 'red' if they have $g - r$ within 0.05 of the peak of the red galaxy $g - r$ distribution specified by Skibba & Sheth (2009), for their observed M_r, again see WCS for more detail.

as well, based on methods of den Hartog & Katgert 1996; Biviano et al. 2006; Wojtak et al. 2007); further details are available in WCS. We will use the mass measurements by WCS via these methods, taking cylinders of radius r_{180b} when a radius choice is required. Just as in that work, lines of sights for clusters are removed when a more massive cluster has its centre within this radius along the observational line of sight.

2.2 Filament finder

We find filaments using an extension of the method described in Zhang et al. (2009). They identify filaments as bridges in dark matter haloes above a threshold halo mass overdensity, of length up to 10 Mpc h^{-1}. It is analogous to the spherical overdensity finder for clusters, where the cluster radius is taken to be that where the average density around the central point drops below some threshold; here the filament radius is where the average density along the cylinder axis drops below some threshold. Just as there are many different halo finders, there is no unique filament finder or definition. This finder is but one of many different ones present in the literature, which not only are based upon such bridge-like definitions, but also include finders constructed around filtering procedures, potential or density gradients, dynamical information and more (see Zhang et al. 2009 for some comparisons between their finder and others). Even for a given filament finder, catalogues must often be specified by the finder parameters as well (e.g. smoothing length for density- or potential-based finders, unbinding criteria for dynamically based finders, etc.). We use the parameters given in Zhang et al. (2009).

The algorithm of Zhang et al. (2009) is as follows: haloes are ordered from the most to the least massive. All haloes with mass $\geq 3 \times 10^{10}\,h^{-1}\,\mathrm{M}_\odot$ are included[3]; mass in the following only refers to this halo mass or above. Starting with the most massive halo ('node'), all haloes within 10 Mpc h^{-1} but at least 3 Mpc h^{-1} away in radius (or r_{200c}, if greater, which did not occur in our sample) are considered as potential end points. For each potential end point, the cylinder radius is varied, up to 3 Mpc h^{-1}, to get the highest overdensity of halo matter in the cylinder between the node and potential end point.[4] This maximum density is then compared to a minimum overdensity (five times background matter density in haloes), and if over this minimum, this end point and its radius are kept. If no potential end points have a halo mass density for their filament greater than the minimum overdensity, then the algorithm moves to the next node. Once all such maximal filaments are found for a given node, the filament with the largest density is kept. The filament is then truncated: its new end point is the most massive halo within it, which has at least three other haloes between it and the central node, and which is at least 3 Mpc h^{-1} away from the central node. The all-filament members are then removed from the list of potential future filament members or end points around any node. The end points are not removed from the list of possible end points for other nodes, but are removed from the list of possible end points associated with this node. This procedure is repeated until no more new filaments are found around the node.

As this procedure frequently produces many more filaments than were evident by eye around clusters (sometimes over 30 around a single cluster), we incorporate a growing and merging procedure as well. After finding the filaments of maximum density around a given node, we grow out the filament radii until the average mass density in haloes within the cylinder stretching to the filament end point drops to less than the minimum overdensity, or the maximum 3 Mpc h^{-1} radius is reached. Haloes lying in two or more such extended filaments are assigned to the one whose axis is the closest. Filament end points with length ℓ and a perpendicular distance $d_\perp$ to another (longer) filament's axis such that $d_\perp/\ell < 3/10$ (the maximum width/maximum length in the algorithm) are merged into the longer filament, unless the shorter filament's end point has other filaments extending out of it. (This allows filament radii >3 Mpc h^{-1}.) These new filaments are then given a central axis determined by the centre of mass of the filament; filaments whose end points do not have additional filaments extending out of them and whose end points are within 25° of each other are merged. This is done in the order of closest to most distant pairs; if >2 filaments are within this range, the two closest are merged, then centres of mass are recalculated to see if the remaining filaments are within the minimum distance, and so on. As an example, the two most massive filaments extending from a cluster of mass $2.7 \times 10^{14}\,h^{-1}\,\mathrm{M}_\odot$ are shown in Fig. 1.

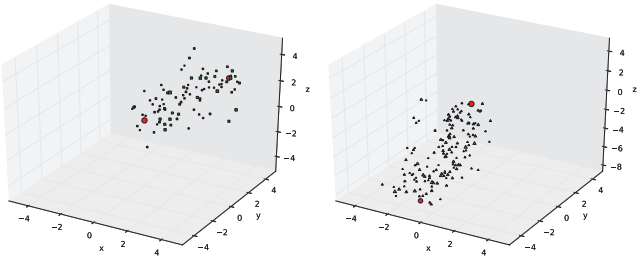

Figure 1. The two largest filaments around a cluster of mass $2.7 \times 10^{14}\,h^{-1}\,\mathrm{M}_\odot$ cluster, after the merging procedure. The central cluster and the two filament end points are shown as large filled circles, other points are other haloes in the filaments. Shown at left are the haloes in the most massive filament ($4.3 \times 10^{13}\,h^{-1}\,\mathrm{M}_\odot$), with a halo of mass $2.4 \times 10^{13}\,h^{-1}\,\mathrm{M}_\odot$ as its end point. At right are the haloes in the second most massive filament ($4.1 \times 10^{13}\,h^{-1}\,\mathrm{M}_\odot$) and the $1.1 \times 10^{13}\,h^{-1}\,\mathrm{M}_\odot$ end point. The units are Mpc h^{-1}. The full distribution of filamentary mass around this cluster is shown in Fig. 4.

The resulting filaments are regions connecting haloes with halo mass overdensity at least five times the background halo mass density, and which are less than 10 Mpc h^{-1} long. The full catalogue at $z = 0.1$ has ∼30 000 filaments and ∼44 000 end points, with 45 per cent of the halo mass fraction in filaments and 36 per cent of the haloes (in number fraction) in filaments. 60 per cent of the $\sim 1.2 \times 10^6$ haloes above the minimum mass cut are either not end points or not in filaments, with the most massive of these having $M = 2.6 \times 10^{12}\,h^{-1}\,\mathrm{M}_\odot$.[5]

Several of the other finders produce filaments which can extend well beyond our 10 Mpc h^{-1} cut-off (e.g. Colberg et al. 2005 found filaments out to 50 Mpc h^{-1}; even longer ones have been found by e.g. Gonzalez & Padilla 2009); some have restrictions on filament nodes (e.g. Colberg et al. 2005 found filaments end only on clusters). Our catalogue has straight filament segments $\leq$10 Mpc h^{-1} in

[3] This is the minimum mass used by Zhang et al. (2009) converted (see White 2001) to our FoF definition.

[4] This radius scale is slightly smaller than that found for galaxy filaments in the 2dGFRS survey (Porter & Raychaudhury 2007; Porter et al. 2008). We thank the referee for pointing this out to us.

[5] Analytic estimates of filamentary mass fractions mentioned above (which use other filament definitions) are not directly comparable because the latter are based upon total mass; mass in haloes above our minimum is only 40 per cent of the mass in the box at $z = 0.1$.

length, built out of dark matter haloes above some minimum overdensity which emanate from clusters and other end points. Longer filaments could presumably be constructed as chains of our shorter ones, augmented by a condition on how much a filament can bend before it is considered instead to be two separate filaments meeting at a node. The length restriction of our finder also affects breakdowns into mass fraction in filaments, nodes and so on, as some of our nodes will instead be filament members if the filaments are extended this way.

The work most similar to ours in focus, studying clusters as filament end points, is Colberg et al. (2005), some related results can also be found and compared in Aragón-Calvo et al. (2010b) (see also Sousbie et al. 2010, who found a cluster as an intersection of filaments in observational data). Colberg et al. (2005) found filaments by looking for matter overdensities by eye between cluster end points, and measured a wide range of filament statistics, including the number of filaments per cluster as a function of mass, stacked filament profiles, length distributions and the fractions of cluster pairs connected by filaments. Aragón-Calvo et al. (2010b) found filaments using a Multiscale Morphology Filter (see their paper for details) and considered similar quantities to Colberg et al. (2005), and in addition introduced a classification for filaments.

3 STATISTICS OF FILAMENTS AROUND CLUSTERS

Our finder is well suited to characterize the local environment of clusters, our target of study here. Of the 243 clusters ($M \geq 10^{14}\,h^{-1}\,\mathrm{M}_{\odot}$) in our box, 227 are also nodes, with ∼1700 filaments. We restrict to these clusters below. Their characteristic radii r_{200c} (radius within which the average enclosed density is 200 times the critical density) range between 0.6 and 1.9 Mpc h^{-1}, i.e. these are not the only extremely rich and massive clusters. The 7 per cent (16) of the clusters which are not nodes are within a filament extending from a more massive cluster, and 15 of the clusters have a cluster within a filament. There are also 41 pairs of clusters within 10 Mpc h^{-1} of each other. We use the term 'connected' filamentary mass to refer to halo mass within a filament connected directly to a cluster, up to and including its other end point.[6] In addition to connected filaments around a cluster, within the 10 Mpc h^{-1} sphere we will also consider all filaments and their end points, all haloes above our minimum mass of $3 \times 10^{10}\,h^{-1}\,\mathrm{M}_{\odot}$ and all galaxies.

In the 10 Mpc h^{-1} spheres surrounding clusters, connected filaments constitute ∼70 per cent of the halo mass on average, but with a very broad distribution of values for individual clusters. A line passing through the 10 Mpc h^{-1} shell centred on a cluster will hit one of the original connected filament cores (from the first step of our algorithm) about 10 per cent of times on average, and one of the grown and merged filaments closer to ∼30 per cent of times, with a wide spread as well. All (not only connected) filaments in this sphere contain closer to ∼90 per cent of the halo mass, with much less cluster-to-cluster scatter. (The unconnected filaments for this cluster go between two other nodes. These other nodes themselves may or may not lie within the 10 Mpc h^{-1} sphere.) In 10 Mpc h^{-1} spheres around 10 000 random points, in comparison, the filaments have a halo mass fraction ranging from 60 to 95 per cent.

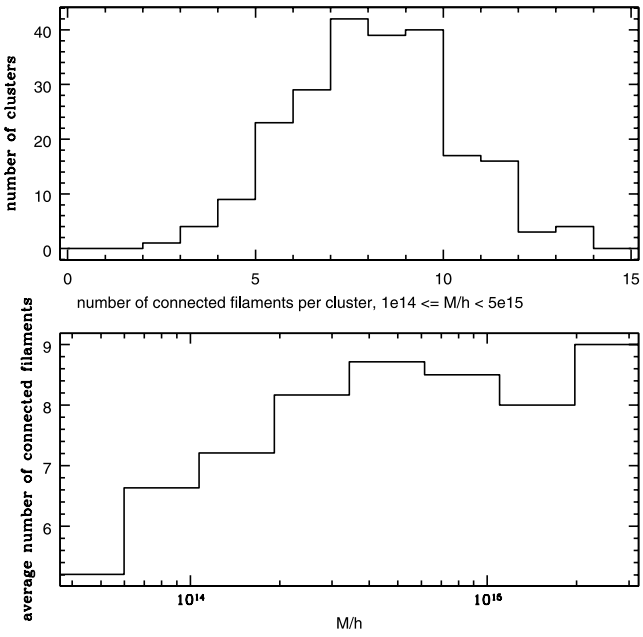

Figure 2. Top: distribution of number of filaments per cluster (haloes with $M \geq 10^{14}\,h^{-1}\,\mathrm{M}_{\odot}$). Bottom: number of filaments as a function of mass for all haloes which are filament end points.

The distribution of the number of connected filaments around clusters, with our finder, is shown at the top of Fig. 2; clusters tend to have 7–9 filaments. We find that more massive haloes have more filaments ending upon them, shown in Fig. 2, bottom, just as found by Colberg et al. (2005) and Aragón-Calvo et al. (2010b) with their different finders.

In addition, connected filaments around clusters tend to be shorter than their counterparts for the much less massive nodes.

The large number of filaments found by the algorithm can be compared to a simplified picture where nodes are fed by a small number of filaments (e.g. three or fewer, Keres et al. 2005, 2009; Dekel et al. 2009). The mass fraction in the largest two or three filaments is substantial, leading to a partial reconciliation of these pictures, as seen in Fig. 3; that is, about half of the clusters have at least ∼75 per cent of their mass in their three largest filaments.

More massive haloes have more filaments around them, more matter in filaments and more matter around them generally, and although the number of filaments for clusters can be quite large, a significant fraction of the filamentary mass is found within the three largest filaments.

4 PLANAR GEOMETRY AROUND CLUSTERS

Filaments provide an anisotropic environment for galaxy clusters. Some approximate trends in the filamentary distribution are accessible via the inertia tensor of its mass, even though filaments are not expected to fill out an ellipsoid. For connected filaments attached to our clusters, the middle eigenvalue of the inertia tensor tends to be smaller than that for the clusters, so that the filament distribution

[6] The finder, even with modifications, still produced some configurations which we modified with post-processing. For example, sometimes a filament would be found with a large 'gap' in the centre, where the gap is due to a previously found filament between two other clusters which crosses the region. Even with this gap, the new filament is above our overdensity threshold. As the previous and new filaments seem to be joined and perhaps one object, we added all the mass (within 10 Mpc h^{-1}) of any previously found filament that came within 3 Mpc h^{-1} to the connected filamentary mass of the cluster; this happened for <10 of our ∼7000 filaments.

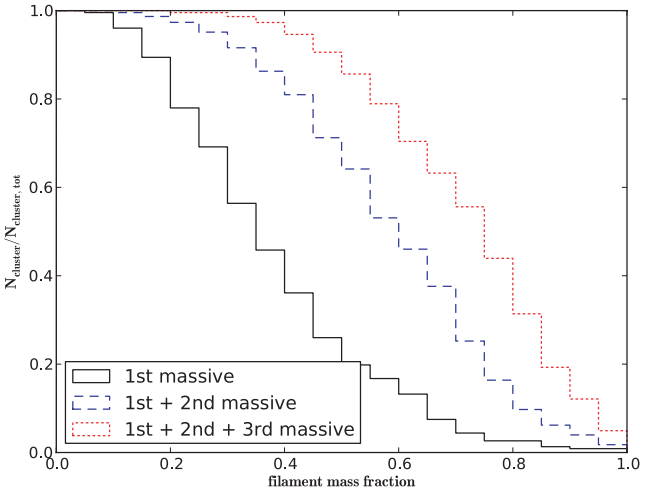

Figure 3. Cumulative fraction of filamentary mass in 1 (solid line), 2 (dashed line) and 3 (dotted line) most massive cluster filaments, as fraction of the number of clusters. For example, about half of the clusters have at least 60 per cent of their connected filament mass in their two largest filaments and at least ∼75 per cent of their mass in their three largest filaments.

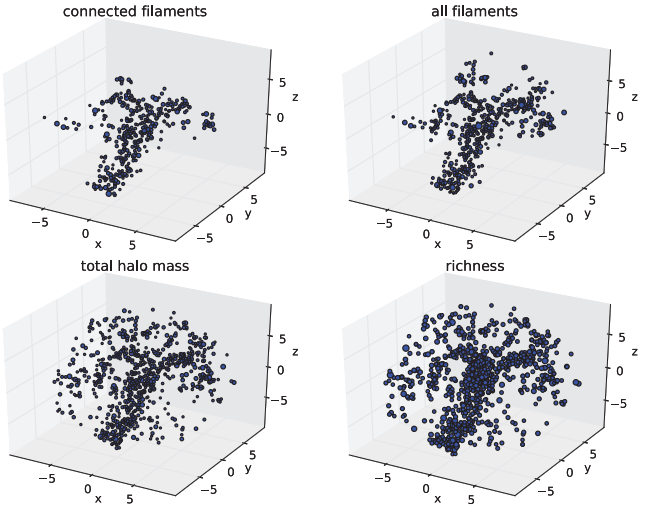

Figure 4. Four types of objects used in constructing planes in a 10 Mpc h^{-1} radius sphere centred on a $2.7 \times 10^{14}\,h^{-1}\,M_\odot$ cluster. Left to right, top to bottom are haloes in connected filaments, haloes in all filaments, all haloes above $3 \times 10^{10}\,h^{-1}\,M_\odot$ mass cut, and galaxies above $0.2L^*$ cut (galaxies in cluster are not shown). Point size is proportional to halo mass or, for richness, halo infall mass (which determines luminosity, see WCS). About 84 per cent of the cluster's connected filament mass is in the connected filament plane.

is 'flatter' than the cluster it surrounds.[7] For reference, the cluster moment of inertia tensors tend to have two relatively large eigenvalues and a smaller one (corresponding to axis ratios $a > b \sim c$, the classic prolate cluster shape; there are many studies of cluster ellipticities, see e.g. Jing & Suto 2002).

The long axis of the cluster has a tendency to lie within the 'flat' directions of the filamentary distribution, and the eigenvector of the cluster's inertia tensor that is perpendicular to the long and middle axes of the cluster (i.e. corresponding to the largest eigenvalue) tends to align with the corresponding direction of the filamentary inertia tensor. (See also van de Weygaert 2006; Aragón-Calvo et al. 2007b; Hahn et al. 2007b; Paz et al. 2008; Aragón-Calvo et al. 2010b; as our nodes will sometimes be members of filaments in other finders, some of these alignments are relevant filament member alignments discussed therein.)

A visual inspection of many of our clusters suggests that the majority of their filamentary mass lies within sheetlike regions, presumably those from which they condensed (see for example some cases illustrated in Aragón-Calvo et al. 2010a, and a discussion of different filament types in Aragón-Calvo et al. 2010b and their 'grid' and 'star' configurations).

To quantify this planarity, we consider four definitions of planes, regions extending ± 1.5 Mpc h^{-1} above and below the central cluster and out to the edge of the local 10 Mpc h^{-1} sphere. We choose their orientations (normals) so that the planes contain the maximum of either (1) connected filament mass, with extra constraints described below; (2) all filamentary mass including end points; (3) total halo mass; or (4) the number of galaxies, within the 10 Mpc h^{-1} sphere. The connected filament mass plane has its normal chosen to be perpendicular to the axes constructed out of a pair of filament end points; this definition has stronger correlations with observables (discussed later) than using pairs of connected filaments without their end points, or using the plane maximizing connected filament mass with no other constraints. The mass in the plane (or richness, when using galaxies) does not include that of the central cluster, as our interest is in the cluster's environment. In Fig. 4 the objects used for these four choices of plane are shown for a cluster of mass $2.7 \times 10^{14}\,M_\odot/h$. It has about 84 per cent of its mass in the connected filament plane.

These four planes tend to have similar orientations, with the all-filament and halo mass planes most often aligned (over 96 per cent clusters have these two normals within 30°). This is not surprising given the dominance of filamentary mass in the 10 Mpc h^{-1} sphere around the cluster noted earlier. For a given cluster, the largest misalignment between any pairs of planes tends to be between its connected filament plane and one of the other planes, which for 15 per cent of the clusters differs by another plane by more than 60°. For most clusters it thus seems that the connected filaments are not as closely aligned with the other planes, which extend further out into the sphere. Plane pairs besides the closely aligned all-filament and halo mass plane have on average 5–10 per cent of the clusters mismatching by >60°.

The mass or richness fractions in these planes is significantly higher than the fraction (∼1/5) of volume which the plane occupies in the sphere. The distribution of connected and total filament mass fractions, in the corresponding planes, for our clusters is shown at the top of Fig. 5, while at the bottom is the distribution for the total halo mass plane. Also shown at the bottom of Fig. 5 is the mass fraction for halo mass planes constructed around 10 000 random points (rescaled to have the same area under the curve), which is smaller on average than around the clusters. The richness fraction, not shown, peaks slightly more sharply than the halo mass fraction, but at a lower fraction (∼60 per cent). For all the plane definitions, 80 per cent of the clusters have more than 60 per cent of their mass (or 55 per cent of their richness) in these planes; about a quarter of

[7] The connected filament distribution becomes more and more cylindrical with decreasing (well below $10^{14}\,h^{-1}\,M_\odot$) central halo mass, with the two largest eigenvalues tending to become equal, and the third becoming smaller and smaller. One reason is that lower mass haloes are expected to be within filaments, rather than to serve as end points; the algorithm used here will tend to break these longer filaments up into more segments as mentioned earlier.

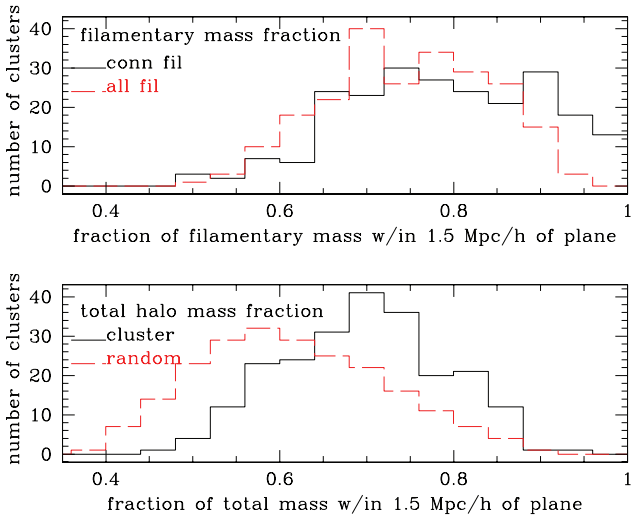

Figure 5. Top: fraction of connected filament mass in connected filament plane (solid) and fraction of all-filamentary mass within the all-filament plane (dashed), both in the fiducial 10 Mpc h^{-1} sphere around clusters. The normals to these planes are within 30° for ∼80 per cent of the clusters. Bottom: the fraction of total halo mass (above our $3 \times 10^{10}\,\mathrm{M}_{\odot}\,h^{-1}$ cut-off) in the mass plane around clusters (solid), and its counterpart around 10 000 random points (dashed, rescaled to have the same number volume as cluster histograms). A large fraction of the filamentary mass and total halo mass in 10 Mpc h^{-1} spheres around clusters resides within this planar region containing ∼20 per cent of the volume.

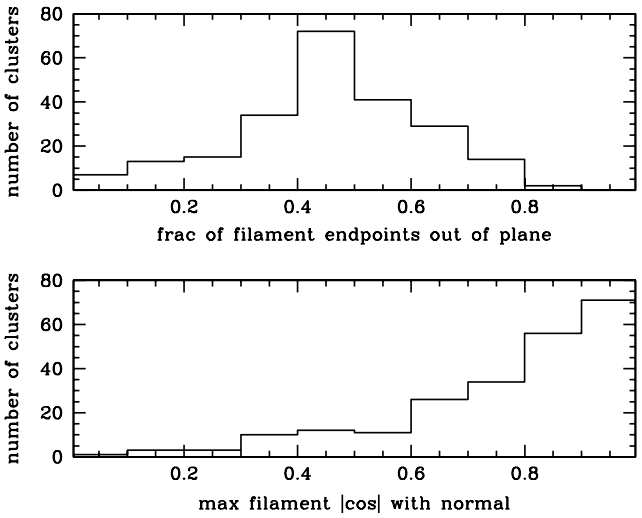

Figure 6. Top: fraction of filament end points lying outside of connected filament plane – many filaments do not have their end points in this plane, even though a large fraction of mass is in this plane (see Fig. 5). Bottom: angle to normal of connected mass plane, for filament closest to the normal; at least one filament tends to be perpendicular to this plane. The corresponding distributions for other planes are similar.

the clusters fell below this fraction for at least one plane definition. Our choice of plane height, ±1.5 Mpc h^{-1} to give 3 Mpc h^{-1} in total, was motivated by the characteristic scale of cluster radii. We explored mass plane heights from 1 to 3 Mpc h^{-1} (total plane widths 2–6 Mpc h^{-1}), and found that the total halo mass fraction scaled as $M_{\rm plane}/M_{\rm sphere} \sim \mathrm{height}^{1/4}$. It would be interesting to understand this scaling in terms of intrinsic filament profiles.

The clusters with large plane misalignments (by >60°) have a low mass or richness fractions, or larger mass within 3 Mpc h^{-1} of the normal of the connected filament plane (but outside of it) almost twice as often as in the full sample (i.e. in ∼2/3 of the clusters with mismatched planes). The misaligned plane clusters have only slightly more often a recent[8] merger or a larger intrinsic cluster flatness (as measured by its inertia tensor); they were equally likely to have other clusters within 10 Mpc h^{-1} as in the full sample.

The connected filament plane's normal, similar to its counterpart for the connected filament's inertia tensor, tends to be aligned with its counterpart for the cluster's mass inertia tensor, and the cluster's long axis is likely to lie in the filament plane. The cluster galaxy positions, have an inertia tensor (setting mass to 1) which appears uncorrelated with this plane. However, restricting to more luminous (>0.4L_*, see WCS for detail) galaxies gives an inertia tensor whose 'most flat' (perpendicular to eigenvector for largest eigenvalue) direction prefers alignment with the normal to the connected filamentary plane, and whose 'long' axis tends to be within the filament plane. The cluster galaxy velocity dispersions can also be given an 'inertia tensor' after subtracting off the average velocity. The alignments of this tensor are more correlated (e.g. Kasun & Evrard 2005; White et al. 2010) with the inertia tensor of the cluster itself than with that of the plane.

Not all filaments lie in these planes. Filamentary mass can extend outside of the plane, as mentioned earlier, as can filament end points. The fraction of filament end points lying outside the connected filament plane is shown in Fig. 6; note that this does not preclude a significant amount of the filament's mass lying within the plane. There is also an increased likelihood for at least one end point to lie perpendicular to the connected plane, as shown in Fig. 6 bottom. The distributions in Fig. 6 are similar for the other plane choices. About 1/10 of the clusters have more than ∼3 per cent of their connected filamentary mass within a 3 Mpc h^{-1} radius of the normal to their plane but above or below the plane itself, which we refer to as perpendicular filaments below. In addition, 10 clusters have over 15 per cent of their mass in a region within 6 Mpc h^{-1} radius of the normal, but outside the connected plane.

As noted earlier (Fig. 3), the two most massive connected filaments often do possess a large fraction of the connected filament mass. The plane defined by these two filaments coincides with the connected filamentary mass plane almost half the times.[9] For 1/3 of the clusters, however, less than half of the connected filament planar mass comes from these two most massive segments. So although the two most massive segments have a preponderance of filamentary mass (Fig. 3), their large mass is not wholly responsible for the dominance of planar structure.

The persistence of the locally defined planes to larger radii can be studied by fixing the plane height and orientation, and extending the plane out into a region of 20 Mpc h^{-1} in radius, and calculating the fractional mass in this larger plane within the larger sphere. The plane volume fraction of the sphere volume drops by about one-half compared to its value in the 10 Mpc h^{-1} sphere, but the (all) filamentary mass, halo mass and richness fractions in their respective planes drop by even more, by a factor of ∼40 per cent. There are filamentary, mass or richness planes in this larger sphere of the same

[8] Specifically, a satellite which has fallen into the cluster within the last time-step, ∼600 Myr, which had at the earlier time at least 1/10 of the cluster's final mass at $z = 0.1$.

[9] We thank G. Jungman for asking us to measure this.

$\pm 1.5\,\mathrm{Mpc}\,h^{-1}$ width which have more of the filamentary, mass or richness in them (and usually more than 1/2 the mass fraction of those defined within $10\,\mathrm{Mpc}\,h^{-1}$). These $20\,\mathrm{Mpc}\,h^{-1}$ filament and mass planes differ from their counterparts at $10\,\mathrm{Mpc}\,h^{-1}$ by over 30° (60°) one-half (one-quarter) of the times, with slightly smaller fractions for the corresponding richness plane.

We did not find a more useful measure of isotropy in the plane (i.e. in the angular direction), although the moment of inertia tensor can indicate how much the planar geometry tends to cylindrical [related questions have been explored when classifying filaments, e.g. Aragón-Calvo et al. (2010b) note a 'star' geometry for sets of filaments]. One possible consequence of isotropy, or its lack, in the plane will be discussed in the next section on mass measurements.

In summary, as has been known, the mass around clusters tends to lie in filaments, which themselves tend to lie within sheets. We have taken a set sheet-width centred on the cluster and maximized different quantities (filament mass, connected filament mass, total halo mass and galaxy richness) within a $10\,\mathrm{Mpc}\,h^{-1}$ sphere around each cluster. The resulting planes are not always aligned: the all-filament and all-halo mass planes are most likely to be aligned, and the largest disagreement between planes for any cluster is most likely to be between the connected filament plane and another plane. The long axis of the cluster tends to lie in the plane as well. Often a perpendicular filament is also present relative to the plane, with others also partially extending out of the sheet. The rough cartoon of the filament shape around clusters is a planar structure with a few filaments sticking out, with a tendency for at least one filament to be close to the plane's normal direction.

5 CORRELATED MASS SCATTER WITH LOCAL FILAMENTARY PLANES

There are observable consequences of the filaments surrounding galaxy clusters: most cluster observations, aside from X-ray,[10] will tend to include some of the cluster environment as well as the cluster itself. We saw above that the majority of the clusters have a preferred direction in their local ($10\,\mathrm{Mpc}\,h^{-1}$ radius) environments, with a large fraction of their surrounding (connected or all-filamentary, or total halo) mass or richness lying in a $3\,\mathrm{Mpc}\,h^{-1}$ sheet. The relation of this local structure to observables can be studied by using the mock observations described in WCS. In that work, cluster masses were measured along 96 lines of sight, using six methods mentioned earlier: two richnesses, Compton decrement, weak lensing and two velocity dispersions. For individual clusters, WCS found correlated outliers in the mass-observable relation along different lines of sight. (It should be noted that Compton decrement and weak lensing both can have significant contamination from beyond the $250\,\mathrm{Mpc}\,h^{-1}$ path measured within the box, so correlation with the local environment is likely smaller than found in WCS and below.) Some connection with environment or intrinsic properties is seen: for the 8 per cent of cases where at least two observables had a large ($\geq$50 per cent) deviation in mass from that predicted by the mean relation, an excess of nearby galaxies from massive or less massive haloes and/or substructure [as detected by the Dressler–Shectman (Dressler & Shectman 1988) test[11]] were found relative to the population without these outliers. ('Nearby' in this context was taken to be within $3\sigma_{\rm kin}$ along the line of sight, where $\sigma_{\rm kin}$ was the velocity dispersion calculated via the prescription described in WCS to remove interlopers, following den Hartog & Katgert 1996; Biviano et al. 2006; Wojtak et al. 2007.)

The filamentary structures and mass planes, and the mass fraction in them, provide an additional characterization of individual cluster environments. The WCS mock observations along the 96 lines of sight of each cluster can now be compared to $|\cos\theta|$, where θ is the angle between the line of sight and the normal to these planes. In addition to the normal to four of the planes mentioned above (connected filament mass, filamentary mass, halo mass and galaxy richness above $0.2L_*$), we also consider a fifth preferred direction, the angle to the nearest filament, and in this case use $|\sin\theta_{\rm fil}|$ of this angle (i.e. $|\cos\theta|$ of the associated normal to the nearest filament).

The rough expectation is that a cluster's measured mass along the sheet with the most filamentary mass or total halo mass ($|\cos\theta| \sim 0$) will be larger than that along the plane's normal vector. This correlation is not expected to be perfect, as there is often a filament close to the normal, and the fraction and distribution of mass in the plane can vary. In particular, the planes are not necessarily completely filled, and some directions through this plane might not intersect large amounts of mass (i.e. there might be a lack of isotropy in the plane as mentioned earlier). For planes which are not isotropically filled, one might thus expect a triangular distribution of mass prediction (on the x-axis) versus $|\cos\theta|$ (on the y-axis): with low mass values for all $|\cos\theta|$, and high mass values for small $|\cos\theta|$ (along the plane). In addition, planes were defined only within $10\,\mathrm{Mpc}\,h^{-1}$ of the cluster, or less: for mass measurements, interlopers sometimes at 10 times or more of that distance can induce scatter. These factors suggest that the alignment of an observational direction with a sheet may not be highly noticeable in observations, even if most of the local (filamentary and/or halo) mass lies within this sheet.

Even with these contraindications, for many clusters we found a strong correlation for many mass measures with the angle between the line of sight and the locally defined planes. These strong correlations are seen not only for both measures of richness, which in principle are closely localized to the cluster, but also for weak lensing, and to a lesser extent, SZ. Correlations are both less frequent and less strong for velocity dispersions. We show an example of one cluster's mass scatter for the six observables in Fig. 7. The measured mass is calculated using scaling from the mean mass–observable relation for clusters in the simulation with $M \geq 10^{14}\,h^{-1}\,\mathrm{M}_\odot$, and its value is shown versus $|\cos\theta|$, where θ is the angle between the observational direction and the connected filament plane's normal. The six panels show two richnesses, SZ, weak lensing and two velocity dispersions. This $2.7 \times 10^{14}\,h^{-1}\,\mathrm{M}_\odot$ cluster, with nine filaments, exhibits strong correlations for all six measurements. It has 84 per cent of its connected filament mass and 72 per cent of its halo mass in the connected filament plane.

Given the noisiness of the data, we are mostly interested in general qualitative trends for the full set of 227 cluster nodes. We estimate correlations for each cluster in two ways. One is to use the correlation coefficient for $(\log M, |\cos\theta|)$, or the truncated set of points by the procedure described below, if that gives a lower absolute value (i.e. weaker value) for the correlation coefficient. These are shown for our example in Fig. 7 above. By eye, a correlation of < -0.25 appears to be a strong correlation, between -0.25 and 0.25 is often (not always) extremely noisy, and a correlation >0.25 indicates an (unexpectedly) positive correlation. We use this division hereon. A positive correlation is unexpected as this means that measured

[10] X-ray structure might have some correlation as well, inasmuch as X-ray substructure is related to filaments which provide the cluster's infalling material.

[11] Within a radius r_{180b}, i.e. within which the average overdensity is 180 times the background density.

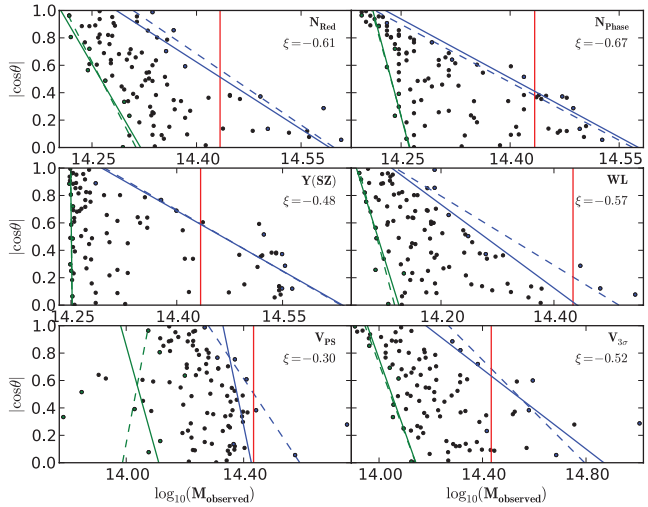

Figure 7. Example of mass scatter correlations: each point is a mass measurement for the same cluster along one of ∼96 lines of sight, having angle θ with the normal of the connected filament plane. The vertical line gives the true mass. The mass measurements are based upon (left to right, top to bottom): red galaxy richness [MaxBCG (Koester et al. 2007) algorithm, for colour assignment description see text]; phase-space richness (galaxies 'in' or 'out' of cluster using criteria of Yang et al. 2008); Compton decrement; weak lensing; phase-based velocity dispersions; and 3σ clipping velocity dispersions. The mass axes for each measurement vary to cover the range of masses found for that technique; note that the scales differ. Envelopes are fit to truncated sets of these points, both using a chi-squared fitting (dashed line) and a shortest perpendicular distance to the envelope (solid line), as described in the text. Where the two severely disagree (e.g. lower left-hand box), one or both fits are bad. The correlation coefficients between $|\cos\theta|$ and $\log_{10} M\,h^{-1}$ are shown at upper right; they are the smallest absolute values of those either for all points or for the truncated set of points. The cluster has mass $2.7 \times 10^{14}\,\mathrm{M}_\odot\,h^{-1}$, nine filaments and about 84 per cent of its connected filament mass in the connected filament plane.

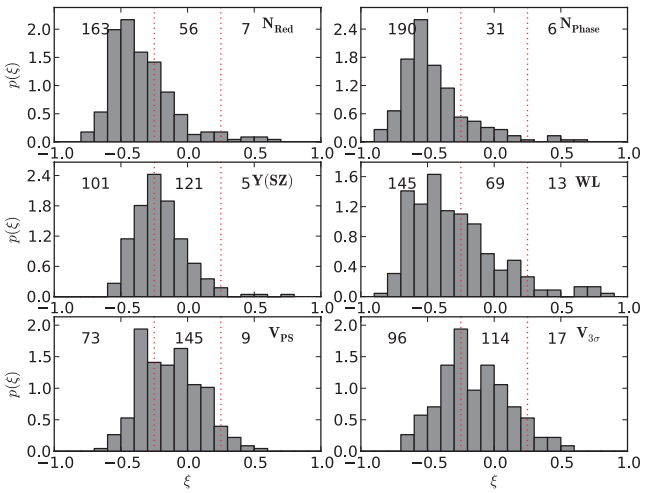

Figure 8. Distributions of correlations between measured mass and $|\cos\theta|$ for the 227 cluster nodes, for six observables. Here θ is the angle between the line of sight and the normal to the connected filament plane. The correlation for each cluster is taken to be the one which is minimum in absolute value either for all points or for the truncated (as described in the text) set of points. The mass measurement methods are as in Fig. 7, i.e. left, right, top to bottom are red galaxy richness, phase-space richness, Compton decrement, weak lensing, velocity dispersion using spatial information and 3σ clipping velocity dispersion. Also shown for each method are (left) the number of clusters with correlation <-0.25 (middle), the number of clusters where the correlation's absolute value is less than 0.25 (and thus possibly noise) and (right) the number of clusters where the correlation is >0.25, i.e. both positive and large, indicating a higher mass estimate as the line of sight becomes more perpendicular to the maximal plane. The dashed vertical lines separate these three regions.

cluster mass increases as the line of sight intersects less of the preferred plane.

The distributions of these correlation coefficients, for the respective mass measurements in Fig. 7 and the connected filament plane, are shown in Fig. 8 for all the 227 cluster nodes. Also printed are the number of clusters with strong (negative), noisy and positive correlations for each measurement. The results are similar for all the five choices of plane within the considerable noise.[12] The fraction of clusters having strong negative or positive correlations, split according to type of mass measurement, is shown in Table 1, with ranges shown for the five choices of plane. The composite correlation of $\log M_{\rm true} - \log M_{\rm pred}$ for all the clusters with $|\cos\theta|$ followed similar trends, with a strongest correlation coefficient for both richnesses, then weak lensing; velocity dispersions and SZ are all similarly low. The amount of correlation between line of sight and normal to various planes is correlated to some extent with the fraction of mass or richness in these planes, as might be expected. There is also a correlation between the strength of correlations of $(\log M, |\cos\theta|)$ and the alignments between planes for each cluster (not surprisingly, this depends upon the pair of planes being considered and the plane used to defined θ). Considering multiwavelength measurements together for each cluster, ∼40–50 per cent of the clusters have a strong negative correlation (i.e. the expected sign) for at least three observables.

For the planes, the correlation coefficient sometimes is low, even with a visible trend of measured mass versus $|\cos\theta|$. One apparent cause is the expected triangular envelope for the points described above. To identify this pattern, we considered slopes of approximate envelopes of the distributions, shown in Fig. 7. Points are binned in eight approximately equally filled[13] $|\cos\theta|$ bins, in each bin $\leq$2 points are discarded at large or small $\log M$ if separated from their nearest neighbour by more than six times the median separation in mass in that bin (or the minimum separation if the median is zero). This threw out many of the notable outliers. It also sometimes threw out other points, in a binning-dependent way, but the number of these points is small and not a concern as we are interested in the average overall properties. Points within 3σ of the median $\log M$ are then kept within each $|\cos\theta|$ bin. Straight line envelopes were then fit to both ends of each bin, either by minimizing perpendicular distance to the envelope or minimizing the chi-squared [note of $\log M(|\cos\theta|)$]. Envelopes for both methods are shown in Fig. 7,

[12] Relative to the connected filament plane shown, all other planes have more strong negative correlations for the two richness-based masses; for planes besides the plane perpendicular to then nearest filament (which is lower), there are more strong correlations for weak lensing and Compton decrement, and similar numbers for velocity dispersions. The plane perpendicular to the nearest filament has fewer negative correlations for weak lensing and Compton decrement and much fewer for velocity dispersions. For all the six mass measurements, the median correlation for the plane perpendicular to the nearest filament is weaker (i.e. more positive) than for the other four planes, by more than the scatter between the median correlations for the other four.

[13] As mentioned earlier, lines of sight where a more massive cluster is present within r_{180b} are discarded.

Table 1. Cluster fractions with strongly negative (expected, rounded to the nearest 5 per cent) and positive (unexpected, not rounded) correlation coefficients between $|\cos\theta|$ and measured mass, by observable, for filament planes, and the effect of also considering the inverse slope of the right-hand ('rh') envelopes of the ($\log M$, $|\cos\theta|$) relation, when either strongly negative (expected) or positive (unexpected), and for directions associated with cluster inertia tensor. The range of values encompass those for planes defined with connected filament mass, all-filamentary mass within $10\,\mathrm{Mpc}\,h^{-1}$ sphere, all-halo mass within $10\,\mathrm{Mpc}\,h^{-1}$ sphere, galaxy richness and the plane whose normal is perpendicular to the filament nearest to the line of sight. Also shown for planes are fractions of clusters with badly defined envelopes ('ill-defined slopes' – suggesting no correlation). The range for strongly negative correlations with two directions of the inertia tensor of the cluster itself (long axis of cluster, using $\sin\theta$, or direction of eigenvector with largest eigenvalue) is also shown; see below in text.

Property	Red richness (per cent)	Phase rich (per cent)	SZ (per cent)	Weak lensing (per cent)	Phase v (per cent)	3σ v (per cent)
corrln < -0.25	70–80	85–90	35–50	55–75	20–40	25–40
corrln < -0.25 or neg rh slope	75–85	85–95	40–55	65–75	25–40	30–40
inertia corrln < -0.25	80–85	75–80	40–50	>90	35–45	55
corrln >0.25	≤ 3	≤ 3	≤ 2	1–6	1–5	2–7
corrln >0.25 or large rh pos slope	1–4	2–5	≤ 3	4–10	4–9	2–7
ill-defined slopes	5	~ 0	~ 0	~ 0	45–50	50–60

the cases shown where they strongly disagree correspond to one or both envelopes having bad fits. From hereon we restrict to envelopes based upon minimizing the perpendicular distance to the envelope. The resulting right- and left-hand inverse slopes are correlated with the correlation coefficients of ($\log M$, $|\cos\theta|$), their mean relation gives a correspondence between our correlation coefficient cut-off ± 0.25 and inverse slopes of the envelopes. We explored adding clusters to the negative (or positive) correlation sample which have inverse slopes less than (or more than) the mean value of inverse slope for our correlation coefficient cut-off ± 0.25; the small effect can be seen in Table 1. (Sometimes the mean value had the wrong sign, e.g. for velocity dispersions for some choice of plane, which have large scatter, in this case the cut-off was set to zero.) We strove to be conservative in claiming a correlation, so that our estimates for the strength of these planar orientational effects tend to be lower bounds.

Most of the times the envelopes found by our algorithm are reasonable to the eye, but sometimes they fail catastrophically, and those were caught by the goodness of fit estimator. The catastrophic failures seem to occur when no correlation is apparent between $|\cos\theta|$ and the measured mass, as does an envelope close to vertical (inverse slope close to zero). The goodness of fits are the worst for the velocity dispersions, which have close to half the clusters not allowing good fits for either the left or right envelopes; even when the goodness of fit passes threshold, the envelopes are often close to vertical: i.e. the minimum or maximum velocity dispersion mass is similar either perpendicular to the maximum plane or looking through it.

For the unexpected positive correlations, a positive inverse left envelope slope can be observed by looking down a filament near the perpendicular to the plane (small angle, large mass) and then catching a 'gap' in the plane (large angle, small mass). It is more difficult to derive >0.25 correlations or large positive right-hand envelope inverse slopes (i.e. the largest measured mass closer to the perpendicular to the dominant plane). These do not dominate but are not uncommon: for any choice of plane, $\sim$10–20 per cent of the clusters have at least one observable with strongly positive inverse right-hand slope or correlation (almost half of these are due to velocity dispersions). This dropped to <5 per cent (down to 1 per cent using the plane perpendicular to the nearest filament or richness) when requiring clusters to have at least three observables with either right-hand positive slope or correlation (most often weak lensing and both dispersion measurements).

Restricting to correlations, which are a cleaner and more conservative measurement, there are 45 clusters with a positive correlation for at least one measurement (usually velocity dispersions). These clusters differ from the full sample in having, twice as often as the latter, high fractions of perpendicular mass to the connected filament plane and/or some pair of planes misaligned by 60° or a recent merger (as defined earlier). They also slightly more often have another massive cluster within $10\,\mathrm{Mpc}\,h^{-1}$, low mass or richness fraction in some plane or are flatter (as measured by its inertia tensor, smallest axis/middle axis <0.6). Fewer than a quarter of the clusters with a positive correlation for at least one measurement do not have one of these factors present, and some of these are close to our cutoffs, e.g. have more mass within $6\,\mathrm{Mpc}\,h^{-1}$ (rather than $3\,\mathrm{Mpc}\,h^{-1}$) to the perpendicular to the connected filament plane than most clusters, or planes mismatching by almost 60°. The 'unexplained' strongly positive correlations occur for weak lensing and velocity dispersion mass measurements.[14] Given the complexity of the cosmic web, and the small region we use to characterize the cluster's environment, it is to be expected that our simple cartoon description will not always correlate precisely with observables.

Similar correlations can be calculated using two axes defined from the inertia tensor for the cluster itself: the 'long' axis of the cluster, corresponding to the eigenvector of the smallest eigenvalue of the inertia tensor, and the direction of the eigenvector for the largest eigenvalue of its inertia tensor (pointing orthogonal to the longest and middle axes of the cluster). As mentioned earlier, these directions are correlated with the planes, with the 'long' cluster axis tending to lie within them and the latter direction tending to align with the plane normals. Compared to the five planes above, the median correlation for these two planes with mass scatter is stronger for red galaxy richness, weak lensing and the two velocity

[14] The fewest cases of strongly positive inverse slope or correlation occur for the plane defined using the perpendicular to the nearest filament to line of sight, suggesting that filaments close to the line of sight might be the cause of positive correlations, but again positive correlations did not always occur for these configurations. However, the plane perpendicular to the nearest filament also gives the fewest (except for richness) strongly negative correlations, i.e. its correlations are weaker in general.

dispersions, is similar for SZ, and brackets that for phase richness (the long axis of the cluster always has the stronger correlation of the two). The strength of effect for the 'long' axis of the cluster is likely due not only to a *plane* being compared to the line of sight, but also to a specific high-density axis within that plane; almost 90 per cent of the clusters have a strong negative correlation for at least three of the six observables. The fractions of strong negative correlations for these two directions determined by the cluster inertia tensor are also shown in Table 1.

In summary, the mass scatter for richness, Compton decrement, weak lensing and velocity dispersion measures is often correlated with the angle to these planes (most for richnesses, and least for velocity dispersions). The correlations are not perfect and can sometimes be weak, or even of the opposite sign than expected. In the latter case it is often also true that the different dominant planes (mass, connected or all-filamentary haloes and richness) are not well aligned, or that a large filament extends perpendicular to the connected filament plane. Besides being correlated with each other, the planes and the mass scatters are also correlated with axes of the cluster's inertia tensor.

6 CONCLUSION

After implementing a filament finder on an N-body simulation, we studied the resulting filamentary environment for the 227 nodes which are also clusters ($M \geq 10^{14}\,\mathrm{M}_\odot\,h^{-1}$). Filaments tend to lie in sheets, presumably those from which they condensed, providing a highly anisotropic environment for the cluster at their centre. Within a $10\,\mathrm{Mpc}\,h^{-1}$ sphere, we identified sheets of width $3\,\mathrm{Mpc}\,h^{-1}$, centred on each cluster, which maximize either total mass, connected filament mass, all-filamentary mass or galaxy richness. The all-filament and halo mass planes are most often closely aligned, while the connected filament plane tends to be within the pair of least aligned planes for the majority of clusters. The direction of the filamentary and mass planes persist slightly as the $10\,\mathrm{Mpc}\,h^{-1}$ spheres are extended to $20\,\mathrm{Mpc}\,h^{-1}$.

We measured the correlation of mass measurement scatters with the direction of observation relative to these planes for mock observations of richness, Compton decrement, weak lensing and velocity dispersions, via correlation coefficients and fits to the envelopes of the measurements. Often there is a strong correlation between measured mass and direction to the local plane, in spite of the relatively small region ($10\,\mathrm{Mpc}\,h^{-1}$ radius) used to define the plane (again, this correlation might be overestimated for Compton decrement and weak lensing, which both can have strong scatter from distances larger than our box size). Strong correlations are least likely for velocity dispersions, and fitting envelopes to their distribution of $|\cos\theta|$ versus $\log M$ tend to fail badly. This is perhaps not surprising because our finder does not include dynamical information. Alignments of observational direction with two of the axes of the inertia tensor of the cluster also result in strong correlations with measured mass scatter.

How these planes and correlations with scatter extends to higher redshift depends upon how the finder extends to higher redshift. This is a subtle question as the finder of Zhang et al. (2009) has a built-in scale: a cut-off for minimum halo mass. A full analysis of appropriate generalizations is beyond the scope of this paper; two natural possibilities, however, are to leave the minimum mass alone, or to choose a minimum mass so that the ratio of the number of haloes to the number of clusters (107 at $z = 0.5$, 25 at $z = 1.0$) remains the same, which gives a minimum mass of $8.2 \times 10^{10}\,h^{-1}\,\mathrm{M}_\odot$ for $z = 0.5$ and $3.0 \times 10^{11}\,h^{-1}\,\mathrm{M}_\odot$ for $z = 1.0$.[15] Choosing the latter case (and luminosity cut at $0.2L^*$), most of the trends persist to these higher redshifts, although the total number of filaments in the box decreases. For $z = 0.5$ and $z = 1.0$, the planar mass fractions around clusters are close to unchanged. For all the three redshifts, there is a slight drop in richness fraction in the richness plane as redshift increases, and the halo mass fraction in planes around random points appears to grow, so that by $z = 1.0$ it is comparable to that around the 25 clusters in the box at $z = 1.0$. For correlations of plane directions with cluster observations, the statistics are very noisy for $z = 1.0$. For $z = 0.5$, the fractions of clusters with strong (expected) negative correlations of angle with plane and mass scatter,[16] as in Table 1, tend to either remain the same in range or slightly increase (velocity dispersions do decrease in one case). In addition, the number of clusters with at least three negative correlations is close to unchanged for three planes, dropping for the richness and nearest filament planes, and positive correlation fractions are about the same except for (an increase for) velocity dispersions. Large plane misalignments are less common, but clusters with misaligned planes still are more likely to have smaller mass fractions in the plane or more perpendicular mass than the full sample.

It would be interesting to determine whether this generalization to higher redshift is appropriate and then to understand the results in terms of the evolution of the filamentary neighbourhood of the clusters and the clusters within them.

The correlations between mass scatter and angle of observation with the planes (and inertia tensor of the cluster) rely upon three-dimensional information available to us as simulators. It would be very interesting to find a way to make this source of mass bias more evident to observers, perhaps by using a filament finder based upon galaxies directly (amongst those mentioned earlier), and seeing how well they trace these planes, or by combining multiwavelength measurements. In-depth studies underway of cluster environments such as Lubin et al. (2009) would be excellent data sets to apply and refine such methods.

ACKNOWLEDGMENTS

We thank Y. Birnboim, O. Hahn, S. Ho, G. Jungman, D. Keres, L. Lubin, S. Nagel, S. Shandarin, A. Szalay, D. Zaritsky and especially M. White for helpful discussions; and we thank M. George, L. Lubin, E. Rozo and the referee for helpful comments on the draft. JDC thanks R. Sheth for an introduction to research on filaments, and the Aspen Center for Physics for providing the place and opportunity for us to meet and discuss. YN thanks the Santa Fe Cosmology School for the opportunity to present this work, and we both thank the participants there for many useful comments and questions, and S. Habib and K. Heitmann for support in order to be able to attend. Martin White's simulations, used in this paper, were performed at the National Energy Research Scientific Computing Center and the Laboratory Research Computing project at Lawrence Berkeley National Laboratory.

REFERENCES

Abell G. O., 1958, ApJS, 3, 211
Altay G., Colberg J. M., Croft R. A. C., 2006, MNRAS, 370, 1422

[15] We thank M. White for this suggestion.
[16] The model for colour assignments is valid only for $z = 0.1$, so we did not consider red galaxy richness at other z.

Aragón-Calvo M. A., Jones B. J. T., van de Weygaert R., van der Hulst J. M., 2007a, A&A, 474, 315
Aragón-Calvo M. A., van de Weygaert R., Jones B. J. T., van der Hulst J. M., 2007b, ApJ, 655, L5
Aragón-Calvo M. A., Shandarin S. F., Szalay A., 2010a, preprint (arXiv:1006.4178)
Aragón-Calvo M. A., van de Weygaert R., Jones B. J. T., 2010b, MNRAS, 408, 2163
Bailin J., Steinmetz M., 2005, ApJ, 627, 647
Barrow J. D., Bhavsar S. P., Sonoda D. H., 1985, MNRAS, 216, 17
Basilakos S., Plionis M., Yepes G., Gottlöber S., Turchaninov V., 2006, MNRAS, 365, 539
Becker M. R., Kravtsov A. V., 2010, preprint (arXiv:1011.1681)
Betancort-Rijo J. E., Trujillo I., 2009, preprint (arXiv:0912.1051)
Bharadway S., Sahni V., Sathyaprakash B. S., Shadarin S. F., 2000, ApJ, 528, 21
Biviano A., Murante G., Borgani S., Diaferio A., Dolag K., Girardi M., 2006, A&A, 456, 23
Bond J. R., Kofman L., Pogosyan D., 1996, Nat, 380, 603
Bond N., Strauss M., Cen R., 2010a, MNRAS, 406, 1609
Bond N. A., Strauss M. A., Cen R., 2010b, MNRAS, 409, 156
Cen R., 1997, ApJ, 485, 39
Chambers S. W., Melott A. L., Miller C. J., 2000, ApJ, 544, 104
Choi E., Bond N. A., Strauss M. A., Coil A. L., Davis M., Willmer C. N. A., 2010, MNRAS, 406, 320
Colberg J. M., 2007, MNRAS, 375, 337
Colberg J., White S. D. M., Jenkins A., Pearce F. R., 1999, MNRAS, 308, 593
Colberg J., Krughoff K. S., Connolly A. J., 2005, MNRAS, 359, 272
Colombi S., Pogosyan D., Souradeep T., 2000, Phys. Rev. Lett. 85, 5515
Conroy C., Gunn J. E., 2010, ApJ, 712, 833
Conroy C., Gunn J. E., White M., 2009, ApJ, 699, 486
Conroy C., White M., Gunn J. E., 2010, ApJ, 708, 58
Costa-Duarte M. V., Sodre Jr L., Durret F., 2010, preprint (arXiv:1010.0981)
Dalton G. B., Efstathiou G., Maddox S. J., Sutherland W. J., 1992, ApJ 390, L1
Davis M., Efstathiou G., Frenk C. S., White S. D. M., 1985, ApJ, 292, 371
de Putter R., White M., 2005, New Astron., 10, 676
De Simone A., Maggiore M., Riotto A., 2010, preprint (arXiv:1007.1903)
Dekel A. et al., 2009, Nat, 457, 451
den Hartog R., Katgert P., 1996, MNRAS, 279, 349
Diaferio A., Geller M. J., 1997, ApJ, 481, 633
Diemand J., Kuhlen M., Madau P., 2006, ApJ, 649, 1
Dolag K., Meneghetti M., Moscardini L., Rasia E., Bonaldi A., 2006, MNRAS, 370, 656
Dressler A., Shectman S. A., 1988, AJ, 95, 985
Einasto J., Klypin A. A., Saar E., Shandarin S. F., 1984, MNRAS, 206, 529
Faltenbacher A., Gottlöber S., Kerscher M., Muller V., 2002, A&A, 395, 1
Faltenbacher A., Allgood B., Gottlöber S., Yepes G., Hoffman Y., 2005, MNRAS, 362, 1099
Faltenbacher A., Li C., Mao S., van den Bosch F. C., Yang X., Jing Y. P., Pasquali A., Mo H. J., 2007, ApJ, 662, L71
Feix M., Xu D., Shan H., Famaey B., Limousin M., Zhao H., Taylor A., 2008, ApJ, 682, 711
Forero-Romero J. E., Hoffman Y., Gottlober S., Klypin A., Yepes G., 2009, MNRAS, 396, 1815
Gal R. R., Lemaux B. C., Lubin L. M., Kocevski D., Squires G. K., 2008, ApJ, 684, 933
Gay C., Pichon C., Le Borgne D., Teyssier R., Sousbie T., Devriendt J., 2010, MNRAS, 404, 1801
Genovese C. R., Perone-Pacifico M., Verdinelli I., Wasserman L., 2010, preprint (arXiv:1003.5536)
Gonzalez R. E., Padilla N., 2009, preprint (arxiv:0912.0006)
Hahn O., Porciani C., Carollo C. M., Dekel A., 2007a, MNRAS, 375, 489
Hahn O., Carollo C. M., Poricani C., Dekel A., 2007b, MNRAS, 381, 4
Hahn O., Teyssier R., Carollo C. M., 2010, preprint (arXiv:1002.1964)
Hallman E. J., O'Shea B. W., Burns J. O., Norman M. L., Harkness R., Wagner R., 2007, ApJ, 671, 27
Hoekstra H., 2001, A&A, 370, 743
Holder G. P., McCarthy I. G., Babul A., 2007, MNRAS, 382, 1697
Hopkins P. F., Bahcall N., Bode N., 2004, ApJ, 618, 1
Jing Y. P., Suto Y., 2002, ApJ, 574, 538
Jones B. J. T., van de Weygaert R., Aragón-Calvo M. A., 2010, MNRAS, 408, 897
Kartaltepe J. S., Ebeling H., Ma C. J., Donovan D., 2008, MNRAS, 389, 1240
Kasun S. F., Evrard A. E., 2005, ApJ, 629, 781
Kereš D., Katz N., Weinberg D. H., Davé R., 2005, MNRAS, 363, 2
Kereš D., Katz N., Fardal M., Davé R., Weinberg D. H., 2009, MNRAS, 395, 160
Koester B. P. et al., 2007, ApJ, 660, 221
Lee J., 2004, ApJ, 614, L1
Lee J., 2006, preprint (astro-ph/0605697)
Lee J., Evrard A. E., 2007, ApJ, 657, 30
Lee J., Springel V., 2010, JCAP, 05, 031
Lee J., Springel V., Pen U.-L., Lemson G., 2008, MNRAS, 389, 1266
Lubin L. M., Gal R. R., Lemaux B. C., Kocevski D. D., Squires G. K., 2009, AJ, 137, 4867
Lumsden S. L., Nichol R. C., Collins C. A., Guzzo L., 1992, MNRAS, 258, 1
Mead J. M. G., King L. J., McCarthy I. G., 2010, MNRAS, 401, 2257
Mecke K. R., Buchert T., Wagner H., 1994, A&A, 288, 697
Meneghetti M., Fedeli C., Pace F., Gottloeber S., Yepes G., 2010, A&A, 519, 90
Metzler C., White M., Loken C., 2001, ApJ, 547, 560
Murphy D. N. A., Eke V. R., Frenk C. S., 2010, preprint (arXiv:1010:2202)
Novikov D., Colombi S., Doré O., 2006, MNRAS, 366, 1201
Onuora L. I., Thomas P. A., 2000, MNRAS, 319, 614
Pandey B., Somnath B., 2006, MNRAS, 372, 827
Paz D. J., Stasyszyn F., Padilla N. D., 2008, MNRAS, 389, 1127
Pereira M. J., Bryan G. L., Gill S. P. D., 2008, ApJ, 672, 825
Pimbblet K. A., 2005a, MNRAS, 358, 256
Pimbblet K. A., 2005b, Publ. Astron. Soc. Australia, 22, 136
Pimbblet K. A., Drinkwater M. J., Hawkrigg M. C., 2004, MNRAS, 354, L61
Poggianti B. M., De Lucia G., Varela J., Aragón-Salamanca A., Finn R., Desai V., von der Linden A., White S. D. M., 2010, MNRAS, 405, 995
Pogosyan D., Pichon C., Gay C., Prunet S., Cardoso J. F., Sousbie T., Colombi S., 2009, MNRAS, 396, 635
Porter S. C., Raychaudhury S., 2005, MNRAS, 364, 1387
Porter S. C., Raychaudhury S., 2007, MNRAS, 375, 1409
Porter S. C., Raychaudhury S., Pimbblet K. A., Drinkwater M. J., 2008, MNRAS, 388, 1152
Ragone-Figueroa C., Plionis M., 2007, MNRAS, 377, 1785
Reblinsky K., Bartelmann M., 1999, A&A, 345, 1
Sahni V., Sathyaprakash B. S., Shandarin S. F., 1998, ApJ, 495, L5
Schäfer B. M., 2009, Int. J. Modern Phys. D, 18, 173
Schmalzing J., 1998, in Mueller V., Gottloeber S., Muecket J. P., Wambsganss J., eds, Proc. 12th Potsdam Cosmology Workshop. p. 195
Schmalzing J., Buchert T., Melott A. L., Sahni V., Sathyaprakash B. S., Shandarin S. F., 1999, ApJ, 526, 568
Shadarin S. F., 2004, preprint (astro-ph/0405303)
Shandarin S., 2010, preprint (arXiv:1011.1924)
Shandarin S. F., Zel'dovich Ia. B., 1983, Comments Astrophys., 10, 33
Shandarin S. F., Sheth J. V., Sahni V., 2004, MNRAS, 353, 162
Shandarin S. F., Habib S., Heitmann K., 2009, preprint (arXiv: 0912.4471)
Shaw L. D., Holder G. P., Bode P., 2008, ApJ, 686, 206
Shen J., Abel T., Mo H. J., Sheth R. K., 2006, ApJ, 645, 783
Sheth J. V., Sahni V., Shandarin S. F., Sathyaprakash B., 2003, MNRAS, 343, 22
Skibba R. A., Sheth R. K., 2009, MNRAS, 392, 1080
Song, H, Lee J., 2010, preprint (arXiv:1006.4101)
Sousbie T., 2010, preprint (arXiv:1009.4015)
Sousbie T., Pichon C., Courtois H., Colombi S., Novikov D., 2008a, ApJ, 672, L1

Sousbie T., Pichon C., Colombi S., Novikov D., Pogosyan D., 2008b, MNRAS, 383, 1655
Sousbie T., Colombi S., Pichon C., 2009, MNRAS, 393, 457
Sousbie T., Pichon C., Kawahara H., 2010, preprint (arXiv:1009.4014)
Splinter R. J., Melott A. L., Linn A., Buck C., Tinker J., 1997, ApJ, 479, 632
Stoica R. S., Martínez V. J., Mateu J., Saar E., 2005, A&A, 434, 423
Stoica R. S., Martinez V. J., Saar E., 2007, Appl. Statist. 56, 459
Stoica R. S., Martinez V. J., Saar E., 2009, preprint (arXiv:0912.2021)
Sunyaev R. A., Zel'dovich Ya. B., 1972, Commun. Astrophys, Space Phys., 4, 173
Sunyaev R. A., Zel'dovich Ya. B., 1980, ARA&A, 18, 537
Tanaka M., Finoguenov A., Kodama T., Koyama Y., Maughan B., Nakata F., 2009, A&A, 505, L9
Tormen G., 1997, MNRAS, 290, 411
van de Weygaert R., 2002, Proc. 2nd Hellenic Cosmology Workshop. p. 153
van de Weygaert R., 2006, preprint (astro-ph/0607539)
van de Weygaert R., Bertschinger E., 1996, MNRAS, 281, 84
van de Weygaert R., Schaap W., 2007, preprint (arXiv:0708.1441)
van de Weygaert R., Vegter G., Platen E., Eldering B., Kruithof N., 2010, preprint (arXiv:1006.2765)
van Haarlem M., van de Weygaert R., 1993, ApJ, 418, 544
van Haarlem M. P., Frenk C. S., White S. D. M., 1997, MNRAS, 287, 817
Voit G. M., 2005, Rev. Modern Phys. 77, 207
Wang H., Mo H. J., Jing Y. P., Guo Y., van den Bosch F. C., Yang X., 2009, MNRAS, 394, 398
Wang H., Mo H. J., Jing Y. P., Yang X., Wang Y., 2010, preprint (arXiv:1007.0612)
Way M. J., Gazis P. R., Scargle J. D., 2010, preprint (arXiv:1009.0387)
White M., 2001, A&A, 367, 27
White M., 2002, ApJS, 143, 241
White R. et al., 1999, AJ, 118, 2014
White M., Hernquist L., Springel V., 2002, ApJ, 579, 16
White M., Cohn J. D., Smit R., 2010, MNRAS, 408, 1818 (WCS)
Wojtak R., Lokas E. L., Mamon G. A., Gottlober S., Prada F., Moles M., 2007, A&A 466, 437
Wray J. J., Bahcall N. A., Bode P., Boettiger C., Hopkins P. F., 2006, ApJ, 652, 907
Wu Y., Batuski D. J., Khalil A., 2009, ApJ, 707, 1160
Yang X., Mo H. J., van den Bosch F. C., 2008, ApJ, 676, 248
Zel'dovich Ia. B., Einasto J., Shandarin S. F., 1982, Nat, 300, 407
Zhang Y., Yang X., Faltenbacher A., Springel V., Lin W., Wang H., 2009, ApJ, 706, 747

This paper has been typeset from a TEX/LATEX file prepared by the author.